GEOPHYSICS, VOL. 79, NO. 4 (JULY-AUGUST 2014); P. L33–L39, 5 FIGS.
10.1190/GEO2013-0216.1

Krauklis wave in a trilayer

Valeri Korneev[1], Ludmila Danilovskaya[2], Seiji Nakagawa[1], and George Moridis[1]

ABSTRACT

The Krauklis wave is a slow dispersive wave mode that propagates in a fluid layer bounded by elastic media. The guided properties of this wave and its ability to generate very short wavelengths at seismic frequency range predict possibility of resonances in fluid-filled rock fractures. Study of Krauklis wave properties at laboratory scales requires evaluation of its propagation velocities in models with finite and thin elastic walls. Analysis of an exact solution for a fluid-filled trilayer with equal thickness plates reveals existence of the Krauklis waves in such a model, as well as another mode which propagates mostly in the solid part. Both propagation modes exist at all frequencies. We derived and verified various asymptotic solutions by comparing their dependencies on layer thicknesses and frequency with the exact numerical solution. Analytical and computational results demonstrate that in a 60-cm-long model, the first resonant frequency can be below 10 Hz. This result suggests that the Krauklis-wave effects can be studied in a laboratory at seismic range of frequencies avoiding a notorious problem of frequency downscaling. Strong dispersive properties of Krauklis waves and their dominant behavior in fluid-fracture systems are likely phenomena explaining the observed frequency-dependent seismic effects in natural underground reservoirs.

INTRODUCTION

Propagation of waves within a trilayer model, in which the central layer is fluid bounded by two elastic plates, is studied numerically by Lloyd and Redwood (1965), who find a low-velocity dispersive propagation mode in such a system. Krauklis (1962) finds and theoretically describes this mode, and it eventually is named after him (Korneev, 2011). The Krauklis wave is a high-amplitude dispersive fluid wave that propagates along a fluid layer, which is of interest for volcanology (Chouet, 1986; Ferrazzini and Aki, 1987; Dunham and Ogden, 2012), hydrofracturing (Ferrazzini et al., 1990; Groenenboom and Fokkema, 1998; Groenenboom and Falk, 2000; Korneev et al., 2009), oil-prospecting geophysics (Goloshubin et al., 1993, 1994), thin-film testing (Coulouvrat et al., 1998), and aural physiology (Bell and Fletcher, 2004; Elliott, 2007). Computations predict the possibility of seismic resonances even in cases involving viscous fluids, such as oil (Korneev, 2008). However, there is as of yet no existing established technology that enables fracture evaluation and monitoring based on the use of Krauklis waves. At laboratory scale, finite wall thickness also becomes a factor that needs to be accounted after. Laboratory measurements would enable studying the effects of fracture-wall roughness and poroelasticity on Krauklis wave propagation, to properly evaluate their contribution in a real field environment. Modeling of Krauklis waves for realistic geometries is a challenging computational problem because such modeling requires using highly variable grids, with grid size inside of a fracture possibly several orders of magnitude smaller than an embedding medium (Frehner and Schmalholz, 2010). Although some asymptotic results for a trilayer model already exist (Coulouvrat et al., 1998; Bell and Fletcher, 2004), they have not yet been compared with exact solutions.

In this paper, we evaluate low-frequency symmetric modes for a trilayer model filled with a nonviscous fluid. Depending on the model parameters, the Krauklis wave can propagate either in "thin-wall" or "thick-wall" regimes. We formulate the conditions for each propagation regime. Numerical evaluations of a set of hypothetical parameters for marble plates suggest the possibility of laboratory resonance excitation for frequencies below 10 Hz, allowing us to study field-scale frequencies at laboratory-scale dimensions.

THEORY

Statement of the problem

Consider a trilayer model (Figure 1), in which a central layer ($j = 1$) with thickness h consists of a nonviscous fluid and two adjacent layers ($j = 2$) are elastic and both have thickness H.

Manuscript received by the Editor 11 June 2013; revised manuscript received 8 October 2013; published online 7 July 2014.
[1]Lawrence Berkeley National Laboratory, Berkeley, California, USA. E-mail: vakorneev@lbl.gov; snakagawa@lbl.gov; gmoridis@lbl.gov.
[2]PGS, Oslo, Norway. E-mail: danilovskaya.luda@gmail.com.

Layers are aligned along the x axis of the x spatial coordinate. The z axis is orthogonal to the layer interfaces, with the origin in the middle of the fluid layer. We are interested in waves propagating along the layer surfaces. The time t dependence of the fields is taken in the form $\exp(-i\omega t)$, with angular frequency ω, and $i = \sqrt{-1}$.

Displacements $\mathbf{u}^{(j)}$ in both layers $j = 1, 2$ obey the equations of motion:

$$(\lambda_j + \mu_j)\nabla\nabla \cdot \mathbf{u}^{(j)} + \mu_j \Delta \mathbf{u}^{(j)} + \omega^2 \rho_j \mathbf{u}^{(j)} = 0 \qquad (1)$$

and can be represented as the sum

$$\mathbf{u}^{(j)} = \mathbf{u}_{\mathrm{P}}^{(j)} + \mathbf{u}_{\mathrm{S}}^{(j)}, \qquad (2)$$

where $\mathbf{u}_{\mathrm{P}}^{(j)}$ and $\mathbf{u}_{\mathrm{S}}^{(j)}$ are compressional and shear components, respectively. These components obey the equations

$$\nabla \times \mathbf{u}_{\mathrm{P}}^{(j)} = 0, \qquad \nabla \cdot \mathbf{u}_{\mathrm{S}}^{(j)} = 0, \qquad (3)$$

and they relate to potentials φ_j and ψ_j through the following equations:

$$\mathbf{u}_{\mathrm{P}}^{(j)} = \nabla \varphi_j, \qquad (4)$$

$$\mathbf{u}_{\mathrm{S}}^{(j)} = \nabla \times (\psi_j \mathbf{y}_1), \qquad (5)$$

where the unit vector along the y axis $\mathbf{y}_1$ is used. The potentials obey the equations

$$\Delta \varphi_j + \frac{\omega^2}{V_{\mathrm{P}j}^2} \varphi_j = 0, \qquad (6)$$

$$\Delta \psi_j + \frac{\omega^2}{V_{\mathrm{S}j}^2} \psi_j = 0, \qquad (7)$$

describing the longitudinal (P-) waves with velocities

$$V_{\mathrm{P}j} = \sqrt{\frac{\lambda_j + 2\mu_j}{\rho_j}}, \qquad (8)$$

and shear (S-) waves with velocities

$$V_{\mathrm{S}j} = \sqrt{\frac{\mu_j}{\rho_j}}, \qquad (9)$$

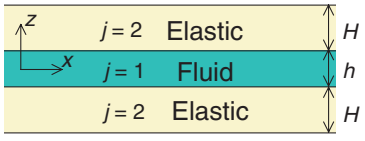

Figure 1. Trilayer model geometry.

expressed through Lamé constants λ_j, μ_j, and density ρ_j, where $(j = 1, 2)$. For the fluid layer $\mu_1 = 0$, and correspondingly, $\psi_1 = 0$.

We consider the wave modes, which are symmetrical with respect to the central axis of the fluid layer and propagate along the interfaces with the (real and positive) wavenumbers $k_x = \omega/V$, where V is the propagation phase velocity. In such a case, the potentials have the forms

$$\varphi_1 = A_1 \left(e^{k_x \sqrt{1-\alpha_{\mathrm{P1}}^2} z} + e^{-k_x \sqrt{1-\alpha_{\mathrm{P1}}^2} z} \right) e^{\mathrm{i} k_x x}, \qquad (10)$$

for the fluid layer, and

$$\varphi_2 = \left(A_2^{(1)} e^{-k_x \sqrt{1-\alpha_{\mathrm{P2}}^2}(z-h/2)} + A_2^{(2)} e^{k_x \sqrt{1-\alpha_{\mathrm{P2}}^2}(z-h/2-H)} \right) e^{\mathrm{i} k_x x}, \qquad (11)$$

$$\psi_2 = \mathrm{i} \left(B_2^{(1)} e^{-k_x \sqrt{1-\alpha_{\mathrm{S2}}^2}(z-h/2)} + B_2^{(2)} e^{k_x \sqrt{1-\alpha_{\mathrm{S2}}^2}(z-h/2-H)} \right) e^{\mathrm{i} k_x x}, \qquad (12)$$

for the elastic layers $j = 2$. In equations 10–12, we used the notations

$$\alpha_{\mathrm{P}j} = \frac{\omega}{k_x V_{\mathrm{P}j}} = \frac{V}{V_{\mathrm{P}j}}, \quad \alpha_{\mathrm{S2}} = \frac{\omega}{k_x V_{\mathrm{S2}}} = \frac{V}{V_{\mathrm{S2}}}, \quad (j = 1, 2), \qquad (13)$$

and A_j and B_2 are constants determined by satisfying the boundary conditions

$$u_z^{(1)} = u_z^{(2)}, \quad \text{at } z = h/2, \qquad (14)$$

$$t_{zz}^{(1)} = t_{zz}^{(2)}, \quad \text{at } z = h/2, \qquad (15)$$

$$t_{xz}^{(2)} = 0, \quad \text{at } z = h/2, \qquad (16)$$

$$t_{zz}^{(2)} = 0, \quad \text{at } z = h/2 + H, \qquad (17)$$

$$t_{xz}^{(2)} = 0, \quad \text{at } z = h/2 + H, \qquad (18)$$

requiring continuity of the normal component $u_z^{(j)}$ of the displacement field, continuity of the normal component for stress $t_{zz}^{(j)}$, and free-surface conditions for the horizontal stress component $t_{zx}^{(2)}$. Expressions for the fields from equations 14–18 have the forms

$$u_x^{(j)} = \frac{\partial \varphi_j}{\partial x} - \frac{\partial \psi_j}{\partial z}, \tag{19}$$

$$u_z^{(j)} = \frac{\partial \varphi_j}{\partial z} + \frac{\partial \psi_j}{\partial x}, \tag{20}$$

$$\tau_{xz}^{(j)} = \mu_j \left(\frac{\partial u_x^{(j)}}{\partial z} + \frac{\partial u_z^{(j)}}{\partial x} \right), \tag{21}$$

$$\tau_{zz}^{(j)} = (\lambda_j + 2\mu_j) \nabla \cdot \mathbf{u}^{(j)} - 2\mu_j \frac{\partial u_x^{(j)}}{\partial x}. \tag{22}$$

With these choices for fields, if we satisfy boundary conditions at the interfaces $z = h/2$ and $z = h/2 + H$, similar conditions will be automatically satisfied at the other two interfaces $z = -h/2$ and $z = -h/2 - H$.

Velocities of the interface waves propagating along the interfaces of the model are the solutions of the equation that represent the boundary condition:

$$\begin{vmatrix} \sqrt{1-\alpha_{P1}^2}\varsigma^-(\alpha_{P1}) & \sqrt{1-\alpha_{P2}^2} & 1 & -\sqrt{1-\alpha_{P2}^2}e_P & e_S \\ \rho_1 V^2 \varsigma^+(\alpha_{P1})/2\mu_2 & b & \sqrt{1-\alpha_{S2}^2} & be_P & -\sqrt{1-\alpha_{S2}^2}e_S \\ 0 & \sqrt{1-\alpha_{P2}^2} & b & -\sqrt{1-\alpha_{P2}^2}e_P & be_S \\ 0 & be_P & \sqrt{1-\alpha_{S2}^2}e_S & b & -\sqrt{1-\alpha_{S2}^2} \\ 0 & \sqrt{1-\alpha_{P2}^2}e_P & be_S & -\sqrt{1-\alpha_{P2}^2} & b \end{vmatrix} = 0, \tag{23}$$

for the vector of unknowns $A_1, A_2^{(1)}, B_2^{(1)}, A_2^{(2)}, B_2^{(2)}$, where

$$\varsigma^{\pm}(\alpha_{P1}) \equiv e^{k_x \sqrt{1-\alpha_{P1}^2} \frac{h}{2}} \pm e^{-k_x \sqrt{1-\alpha_{P1}^2} \frac{h}{2}}, \tag{24}$$

$$e_P \equiv e^{-k_x \sqrt{1-\alpha_{P2}^2} H}, \tag{25}$$

$$e_S \equiv e^{-k_x \sqrt{1-\alpha_{S2}^2} H}, \tag{26}$$

$$b = 1 - \frac{\alpha_{S2}^2}{2} \tag{27}$$

We are searching for the roots of equation 23, which exist at low frequencies, i.e., they can infinitely closely reach the zero frequency. As shown below, there are two such roots, where the first root V_1 corresponds to a mode propagating primarily in the fluid, and the second root V_2 corresponds to a mode propagating primarily in the elastic medium. Both roots are real (no attenuation) and can be found exactly by a numerical grid search method. For the limiting cases of plate thicknesses, the analytic asymptotic solutions can be obtained.

Thick-wall case

When $H \to \infty$, all the matrix elements containing functions e_P and e_S vanish. Then, the upper 3×3 submatrix in equation 23 gives the equation

$$qR\xi_1 - \frac{\alpha_{S2}^2}{2} \sqrt{1-\alpha_{P2}^2} = 0, \tag{28}$$

where

$$R \equiv b^2 - \sqrt{1-\alpha_{S2}^2} \sqrt{1-\alpha_{P2}^2}, \tag{29}$$

$$q = \frac{2\mu_2}{V^2 \rho_1}, \tag{30}$$

$$\xi_1 = \tanh\left(\sqrt{1-\alpha_{P1}^2} \frac{k_x h}{2} \right) \sqrt{1-\alpha_{P1}^2}, \tag{31}$$

for the Krauklis wave with velocity $V_1 \approx V_K$ when plate thicknesses are infinitely large and exponentially decaying surface waves related to a fluid do not interact with the outer boundary. By V_K, we denote an exact solution of the (Krauklis) equation 28.

At low frequencies, when

$$\left| \sqrt{1-\alpha_{P1}^2} \frac{k_x h}{2} \right| < 1, \tag{32}$$

and approximation

$$\tanh(x) \approx x, \tag{33}$$

can be used in equation 28, the Krauklis-wave velocity has the form

$$V_1 \approx V_K \approx V_{K0} \equiv \left(\frac{\omega h \mu_2}{\rho_1} (1-\gamma^2) \right)^{\frac{1}{3}}, \tag{34}$$

where the elastic velocity ratio is $\gamma = V_{S2}/V_{P2}$. Equation 34 describes a thick-wall propagation regime for the Krauklis wave, in which the wave processes in the fluid layer are not affected by the presence of the outer free surfaces $z = \pm(h/2 + H)$.

For the same assumption $H \to \infty$, the lower 2×2 submatrix from expression 23 gives the equation

$$R = 0, \tag{35}$$

for the Rayleigh wave propagating with constant velocity $V_2 \approx V_R < V_{S2}$ along the outer free surface $z = \pm(h/2 + H)$.

At high frequencies, equation 28 takes the form of a Scholte equation:

$$qR\sqrt{1-\alpha_{P1}^2}-\frac{\alpha_{S2}^2}{2}\sqrt{1-\alpha_{P2}^2}=0, \tag{36}$$

which has a nondispersive real solution. Solution V_{Sh} of equation 36 has a slightly lower value than the lowest velocity in the model (V_{S2} or V_{P1}).

Thin-wall case

To derive a low-frequency asymptote for thin plates, we find it convenient to introduce new unknowns:

$$A_S=A_2^{(1)}+A_2^{(2)}, \tag{37}$$

$$B_S=B_2^{(1)}-B_2^{(2)}, \tag{38}$$

and

$$A_A=A_2^{(1)}-A_2^{(2)}, \tag{39}$$

$$B_A=B_2^{(1)}+B_2^{(2)}, \tag{40}$$

which correspondingly describe symmetric and asymmetric field components of the P- and S-fields in elastic layers.

Then, for the vector of unknowns A_1, A_S, B_S, A_A, B_A, we have from equation 23,

$$\begin{vmatrix} q\xi_1 & \xi_2 & \chi_2 & 1 & 1 \\ 1 & 1-\alpha_{S2}^2/2 & 1 & \frac{1-\alpha_{S2}^2/2}{1-\alpha_{P2}^2}\xi_2 & (1-\alpha_{S2}^2)\chi_2 \\ 0 & \xi_2 & (1-\alpha_{S2}^2/2)\chi_2 & 1 & (1-\alpha_{S2}^2/2) \\ 0 & 1-\alpha_{S2}^2/2 & 1 & -\frac{1-\alpha_{S2}^2/2}{1-\alpha_{P2}^2}\xi_2 & -(1-\alpha_{S2}^2)\chi_2 \\ 0 & -\xi_2 & -(1-\alpha_{S2}^2/2)\chi_2 & 1 & (1-\alpha_{S2}^2/2) \end{vmatrix} = 0, \tag{41}$$

where we used the notations

$$\xi_2=\tanh\left(\sqrt{1-\alpha_{P2}^2}\frac{k_xH}{2}\right)\sqrt{1-\alpha_{P2}^2}, \tag{42}$$

$$\chi_2=\tanh\left(\sqrt{1-\alpha_{S2}^2}\frac{k_xH}{2}\right)/\sqrt{1-\alpha_{S2}^2}. \tag{43}$$

Equation 41 can be further simplified to the form

$$\begin{vmatrix} q\xi_1 & \xi_2 & \chi_2 & 1 & 1 \\ 1 & 2-\alpha_{S2}^2 & 2 & 0 & 0 \\ 0 & \xi_2 & (1-\alpha_{S2}^2/2)\chi_2 & 0 & 0 \\ 1 & 0 & 0 & 2\frac{1-\alpha_{S2}^2/2}{1-\alpha_{P2}^2}\xi_2 & 2(1-\alpha_{S2}^2)\chi_2 \\ 0 & 0 & 0 & 1 & (1-\alpha_{S2}^2/2) \end{vmatrix} = 0, \tag{44}$$

giving the following relations:

$$\xi_2A_S+\left(\frac{1-\alpha_{S2}^2}{2}\right)\chi_2B_S=0, \tag{45}$$

$$A_A+\left(\frac{1-\alpha_{S2}^2}{2}\right)B_A=0, \tag{46}$$

which reduce equation 41 to the 3×3 determinant for the unknowns A_1, A_S, A_A:

$$\begin{vmatrix} \frac{2bq\xi_1}{\alpha_{S2}^2} & -\xi_2 & -1 \\ 1 & a_{22} & 0 \\ 1 & 0 & a_{33} \end{vmatrix} = 0, \tag{47}$$

where

$$a_{22}=2\left(b-\frac{\chi_2}{b\xi_2}\right), \tag{48}$$

$$a_{33}=2\left(\frac{b\xi_2}{1-\alpha_{P2}^2}-\frac{(1-\alpha_{S2}^2)\chi_2}{b}\right). \tag{49}$$

Thus, equation 47 can be written in the form

$$q\xi_1a_{22}a_{33}+\xi_2a_{33}+a_{22}=0. \tag{50}$$

Note that equation 50 has the same roots V_1 and V_2 as the original equation 23.

Using expansion 33 for ξ_1 and expansion

$$\tanh(x)\approx x-\frac{x^3}{3}, \tag{51}$$

for the functions ξ_2 and χ_2, from equation 50, we obtain two roots:

$$V_1\approx V_{K0}^*\equiv\left(\frac{\omega^4H^3\mu_2(1-\gamma^2)}{6\rho_1}\right)^{\frac{1}{6}} =\left(\frac{1}{6}\right)^{\frac{1}{6}}\sqrt{\omega HV_K}\approx0.742\sqrt{\omega HV_K}, \tag{52}$$

for the thin-wall asymptote of the Krauklis wave, and

$$V_2 \approx V_L = 2\sqrt{1-\gamma^2}V_{S2} \tag{53}$$

for the symmetric Lamb wave in the elastic plate.

Depending on the parameters, the thick-wall regime may or may not exist for a particular model. This regime occurs when a high-frequency field, although not affected by the outer free surfaces, is still affected by the other interface of the fluid layer. The transition conditions between different regimes are satisfied when the velocities for those regimes are approximately equal (Korneev, 2010). Thus, the Krauklis wave transforms into a Scholte wave when

$$V_{Sh} = V_{K0}, \tag{54}$$

and the transition between a Krauklis wave in the thin-wall regime and a Krauklis wave in the low-frequency regime of two half-spaces occurs when

$$V^*_{K0} = V_{K0}. \tag{55}$$

NUMERICAL RESULTS

We performed computations with a model consisting of a water layer with parameters $V_{P1} = 1500$ m/s, $\rho_1 = 1000$ kg/m^3, between two marble plates with parameters $V_{P2} = 5587$ m/s, $V_{S2} = 3135$ m/s, and $\rho_2 = 2670$ kg/m^3. Figure 2 shows the dispersion curves of phase velocities with their asymptotes as functions of frequency, for the model of a 1-mm-thick fluid layer and 3-cm-thick elastic plates. Shown are the exact solutions V_1 and V_2 obtained by a root grid search for equation 50 and solutions of equations 28, 35, and 36, representing Rayleigh (V_R), Krauklis (V_K), and Scholte (V_{Sh}) waves, respectively. Also shown are the thick-wall (solution V_{K0} of equation 34) and thin-wall (solution V^*_{K0} of equation 53) asymptotes for the Krauklis wave. The transition conditions 54 (I) and 55 (II) are marked by circles. In Figure 3, the same curves are shown as a function of the elastic plate's thickness for a 20-Hz frequency. Figure 4 shows the phase velocity of the Krauklis wave as a function of frequency for fixed values of the elastic plate's thickness. When the thickness of the elastic plates decreases, the phase velocity of the Krauklis wave increases. At the high-frequency limit, the Krauklis wave becomes a nondispersive Scholte wave.

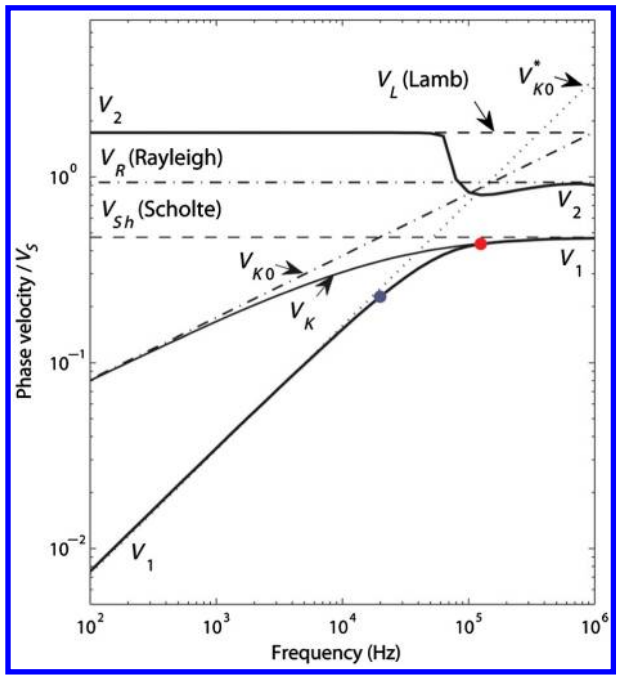

Figure 2. Phase velocities of surface waves in a trilayer with marble plates as functions of frequency. Shown are the solutions V_1 and V_2 of the exact equation 50 and solutions of equations 28, 35, and 36, representing Rayleigh (V_R), Krauklis (V_K), and Scholte (V_{Sh}) waves, respectively. Also shown are the thick-wall (solution V_{K0} of equation 34) and thin-wall (solution V^*_{K0} of equation 53) asymptotes for the Krauklis wave. The blue dot indicates the transition condition 54. The red dot indicates the transition condition 55. Velocities are normalized by the shear velocity.

Predictions of low-frequency resonances were used for a model made of water and marble with a 1-mm-thick fluid layer, 3-cm-thick elastic plates, and 60-cm-long trilayer. We assume rigid conditions for both ends. Resonance conditions for a trilayer with length l:

$$\left(\frac{lf_n}{V_1}\right) = \left(\frac{n+1}{2}\right), \quad n = 0, 1, 2, \ldots \tag{56}$$

assume that at the fracture tips, fluid displacement becomes zero. For the parameters used above, the resonance frequencies for the first three modes are: $f_0 = 6.9$, $f_1 = 178$, and $f_2 = 794$ Hz.

To simulate a propagation of the Krauklis wave excited by a point-pressure source along a center axis of the model, we used OASES software (Schmidt and Tango, 1986; Schmidt, 2004). The fluid layer with 1-mm thickness has parameters $V_{P1} = 1500$ m/s, $\rho_1 = 1000$ kg/m^3, and the elastic plates have parameters $V_{P2} = 4200$, $V_{S2} = 2500$ m/s, and $\rho_2 = 2700$ kg/m^3. Figure 5

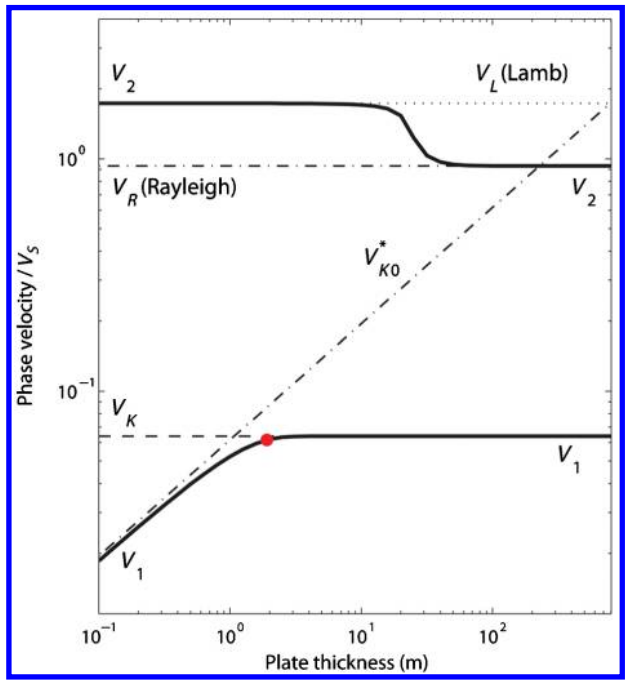

Figure 3. Phase velocities of surface waves in a trilayer with marble plates as functions of plate thickness. Notations are the same as on Figure 2.

shows the dominant horizontal component of the field when the plate thickness is 3 cm (a) and when it is infinite (b). The interval between data points is 5 m. For a Ricker wavelet (a first derivative of the Gaussian bell) with dominant frequency 50 Hz was used. The finite plate case exhibits the stronger dispersion because it follows from equations 52 and 34.

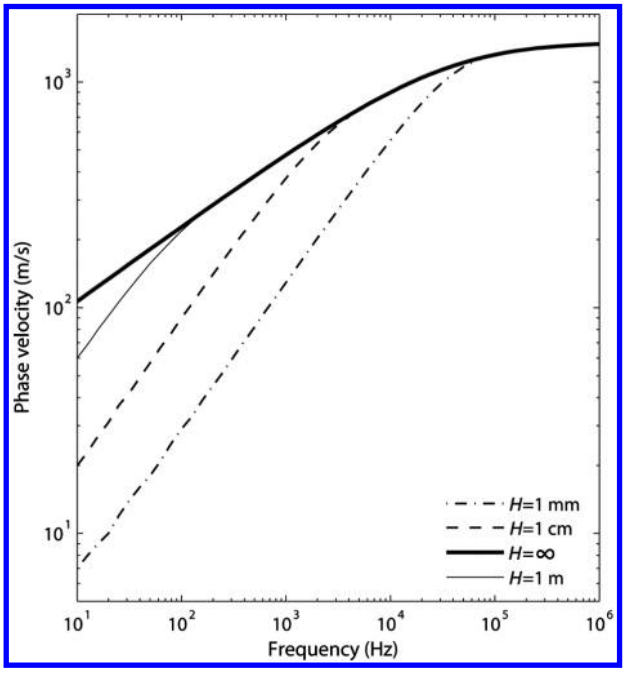

Figure 4. Phase velocities of a Krauklis wave as functions of frequency for different plate thicknesses.

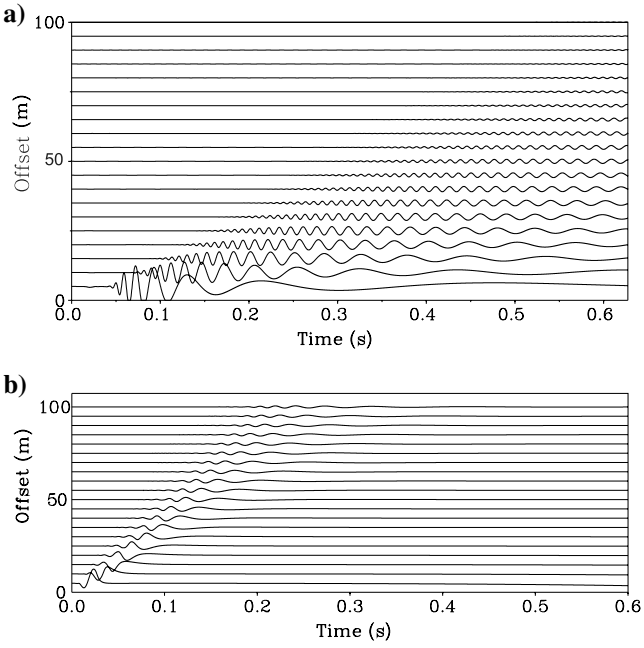

Figure 5. Horizontal component of a full wavefield along a central axis for a trilayer (a) and a model with half-spaces (b).

DISCUSSION

As in the case of alternating fluid-elastic layers (Korneev, 2011), in the trilayer model there are two main modes of propagation for surface waves: (1) primarily in the elastic plates, in the form of a symmetrical Lamb wave for small-plate thickness, and in the form of a Rayleigh wave, when a large enough thickness enables this wave to propagate along the outer surfaces with exponentially decaying amplitude, and (2) primarily in the fluid, in the form of a Krauklis wave with strong dispersion, unless the fluid layer thickness (or high frequency) makes it a nondispersive Scholte wave. The dispersion of a Krauklis wave for finite thin walls is stronger than in a model with elastic half-spaces because of the low compliance of thin plates. Different wave-propagation regimes smoothly interchange at the transition zones described by conditions 54 and 55. Equation 53 can also be derived from equation 8 in Coulouvrat et al. (1998), who use a different analytical approach, assuming an engineering application for adhesive-tape testing. This helped in validation of the derived results.

Krauklis waves are considered to have great potential use in studying fluid-filled fractures because such waves are a main mode of propagation there, with highest amplitude compared with all other waves. Our numerical examples suggest that excitation of Krauklis waves at a seismic range of frequencies is possible at a laboratory scale. This finding solves the notorious problem of frequency downscaling from an ultrasonic range, typically confronted in rock laboratories with field scales. One potential problem in applying the obtained results is in the assumption of infinitely long model walls. In practice, the length of the model will be finite, and the wall's compliance will likely vary along the wall surface, especially at the edges. This problem could then potentially require a more complex analytical or numerical approach.

After successful detection of the Krauklis wave, laboratory studies could potentially expand to more complex and realistic fracture properties and geometries, which are hard to handle using analytical methods.

CONCLUSIONS

Within a trilayer model, the Krauklis wave can propagate in a thin-wall regime with velocities significantly lower than in a model with half-space elastic media. Analytical conditions allow evaluation of the transitions between different asymptotes of the Krauklis wave. At high frequencies, the Krauklis wave becomes a Scholte wave. All obtained asymptotes are verified by comparison with exact solutions. Resonance conditions for the Krauklis wave predict the existence of resonances within seismic frequency range at laboratory scale. If verified, this would allow studies of the Krauklis wave in a variety of realistic models simulating fluid-filled fractures. Strong dispersive properties of Krauklis waves and their dominant behavior in fluid-fracture systems are likely phenomena explaining the observed frequency-dependent seismic effects in natural underground fluid reservoirs.

ACKNOWLEDGMENTS

This work was partially funded through the director of the Office of Science, Office of Basic Energy Sciences, and by the Research Partnership to Secure Energy for America through the Ultra-Deepwater and Unconventional Natural Gas and Other Petroleum

Resources Research and Development Program, as authorized by the U.S. Energy Policy Act of 2005, supported by the assistant secretary for Fossil Energy of the Office of Natural Gas and Petroleum Technology, through the National Energy Technology Laboratory, of the U.S. Department of Energy under contract no. DE-AC02-05CH11231. The comments of C. Morency, K. van Dalen, and an anonymous reviewer helped very much to improve the paper.

REFERENCES

Bell, A., and N. H. Fletcher, 2004, The cochlear amplifier as a standing wave: "Squirting" waves between rows of outer hair cells?: Journal of the Acoustical Society of America, **116**, 1016–1024, doi: 10.1121/1.1766053.

Chouet, B., 1986, Dynamics of a fluid-driven crack in three dimensions by the finite-difference method: Journal of Geophysical Research, **91**, 13967–13992, doi: 10.1029/JB091iB14p13967.

Coulouvrat, F., M. Rousseau, O. Lenoir, and J. Izbicki, 1998, Lamb-type waves in a symmetric solid-fluid-solid trilayer: Acustica, **84**, 12–20.

Dunham, E. M., and D. E. Ogden, 2012, Guided waves along fluid-filled cracks in elastic solids and instability at high flow rates: Journal of Applied Mechanics, **73**, no. 3, 031020, doi: 10.1115/1.4005961.

Elliott, S. J., 2007, Wave propagation in a constrained fluid layer bounded by an elastic half-space and its relevance in cochlear micromechanics: Journal of Sound and Vibration, **305**, 918–924, doi: 10.1016/j.jsv.2007.04.040.

Ferrazzini, V., and K. Aki, 1987, Slow waves trapped in a fluid-filled infinite crack: Implications for volcanic tremor: Journal of Geophysical Research, **92**, 9215–9223, doi: 10.1029/JB092iB09p09215.

Ferrazzini, V., B. Chouet, M. Fehler, and K. Aki, 1990, Quantitative analysis of long-period events recorded during hydrofracture experiments at Fenton Hill, New Mexico: Implications for volcanic tremor: Journal of Geophysical Research, **95**, 21871–21884, doi: 10.1029/JB095iB13p21871.

Frehner, M., and S. Schmalholz, 2010, Finite-element simulations of Stoneley guided wave reflection and scattering at the tips of fluid-filled fractures: Geophysics, **75**, no. 2, T23–T36, doi: 10.1190/1.3340361.

Goloshubin, G. M., P. V. Krauklis, L. A. Molotkov, and H. B. Helle, 1993, Slow wave in oil-saturated layer: 55th Annual International Conference and Exhibition, EAGE.

Goloshubin, G. M., P. V. Krauklis, L. A. Molotkov, and H. B. Helle, 1994, Slow wave phenomenon at seismic frequencies: 63rd Annual International Meeting, SEG, Expanded Abstracts, 809–811.

Groenenboom, J., and J. Falk, 2000, Scattering by hydraulic fractures: Finite-difference modeling and laboratory data: Geophysics, **65**, 612–622, doi: 10.1190/1.1444757.

Groenenboom, J., and J. T. Fokkema, 1998, Guided waves along hydraulic fractures: 67th Annual International Meeting, SEG, Expanded Abstracts, 1632–1635.

Korneev, V. A., 2008, Slow waves in fractures filled with viscous fluid: Geophysics, **73**, no. 1, N1–N7, doi: 10.1190/1.2802174.

Korneev, V. A., 2010, Low-frequency fluid waves in fractures and pipes: Geophysics, **75**, no. 6, N97–N107, doi: 10.1190/1.3484155.

Korneev, V. A., 2011, Krauklis wave in a stack of alternating fluid-elastic layers: Geophysics, **76**, no. 6, N47–N53, doi: 10.1190/geo2011-0086.1.

Korneev, V., A. Ponomarenko, and B. Kashtan, 2009, Stoneley guided waves: What is missing in Biot's theory?: Proceedings of the Fourth Biot Conference on Poromechanics: DEStech Publications Inc., 706–711.

Krauklis, P. V., 1962, About some low frequency oscillations of a liquid layer in elastic medium: PMM, **26**, 1111–1115 (in Russian).

Lloyd, P., and M. Redwood, 1965, Wave propagation in a layered plate composed of two solids with perfect contact, slip, or a fluid layer at their interface: Acustica, **16**, 224–232.

Schmidt, H., 2004, OASES version 3.1 user guide and reference manual: MIT.

Schmidt, H., and G. Tango, 1986, Efficient global matrix approach to the computation of synthetic seismograms: Geophysical Journal of the Royal Astronomical Society, **84**, 331–359, doi: 10.1111/j.1365-246X.1986.tb04359.x.